Dual functions of gold nanorods as photothermal agent and autofluorescence enhancer to track cell death during plasmonic photothermal therapy

Ravi Kumar Kannadorai, Geraldine Giap Ying Chiew, Kathy Qian Luo,

Quan Liu*

School of Chemical and Biomedical Engineering, Nanyang Technological University, Singapore 637457

Corresponding Author: quanliu@ntu.edu.sg

Abstract

Gold nanorods have the potential to localize the treatment procedure by hyperthermia and influence the fluorescence. The longitudinal plasmon peak contributes to the photothermal effect by converting light to heat. When these nanorods are PEGylated, it not only makes it biocompatible but also acts a spacer layer during fluorescence enhancement. When the PEGylated nanorods are internalised inside the cells through endocytosis, the transverse plasmonic peak combined with the enhanced absorption and scattering properties of the nanorods can enhance the autofluorescence emission intensity from the cell. The autofluorescence from the mitochondria inside cells which reflects the respiratory status of the cell was enhanced by two times by the presence of nanorods within the cell. At four minutes the nanorods incubated cells reached the hyperthermic temperature when illuminated continuously with near infrared laser. The cell viability test and autofluorescence intensity curve showed similar trend indicating the progress of cell death over time. This is the first report to the best of our knowledge to suggest the potential of exploiting the dual capabilities of gold nanorods as photothermal agents and autofluorescence enhancer to track the cell death.

Key words: photothermal therapy, hyperthermia, gold nanorods, necrosis, autofluorescence, renal cell carcinoma

1. Introduction

Plasmonic photothermal therapy (PPTT) [1] is getting evolved as an alternative to the traditional laser therapy techniques due to its advantages in exploiting the unique features of metal nanoparticles such as high photostability, reduced photobleaching and enhanced absorption cross-sections as compared to the traditional photothermal agents. The light to heat conversion property of the nanoparticles, particularly gold nanoparticles, is exploited to localize the heating to the desired region in PPTT. Nanoparticles such as nanorods [2-6], nanoshells [7-11], nanostars [12-14] and nanocages [15-18] have plasmon resonance wavelengths in the near infrared (NIR) region which can absorb the NIR laser and produce heat. Since NIR falls within the therapeutic optical window, the tissue is mostly transparent to NIR light thus eliminating the major hindrance due to absorption of laser light by the tissue around the target region during therapy. Plasmonic nanoparticles combined with NIR lasers have been successfully used to treat cancers such as human breast epithelial cancer [8], prostate cancer [19], oral squamous cell carcinoma [3] and colon cancer [20] xenografted into mice by raising the local temperature to the hyperthermic region. Apart from treatment, nanoparticles have the capability to improve cellular imaging due to the enhanced absorption and scattering of electromagnetic radiation particularly in cancer imaging techniques such as dark field microscopy [2, 21], confocal microscopy [22, 23] and electronic microscopy [21, 24].

Treating cancer by hyperthermia is a well established technique which mainly depends on the thermal dosage and exposure time [25]. By just monitoring the temperature rise over time during photothermal therapy one can predict cellular death. Hence in PPTT applications, temperature is used as a common indicator to monitor the outcome of the treatment procedure [3, 26, 27], which is later verified by excising the tumor and performing histopathology [28], or by monitoring its survival rate of the treated animals [29], or by measuring the tumor size over time after therapy [29]. However, the therapeutic procedure with temperature monitoring alone has been found unable to provide the outcome of the treatment during the therapy [30, 31]. The other

alternative is to predict the thermal damage at the cellular level based on the temperature history and exposure time according to Arrhenius law [32]. Thermal damage has been used for treatment planning in numerical studies to calculate the extent of thermal damage [33, 34].

The redox ratio based on tissue autofluorescence measurements, is another potentially more effective indicator of cell death in PPTT, because it directly measures the respiratory status of cells [35-37]. A spectral filtering modulation method [38] can be used to measure both the redox ratio, which indicates the respiratory status, and haemoglobin parameters, which reflects the oxygen supply and consumption from a single fluorescence spectrum. Cellular death can be tracked continuously by measuring fluorescence emitted by endogenous chromophores including nicotinamide adenine dinucleotide (NADH) or flavin adenine dinucleotide (FAD) [36, 39]. This method is an excellent research tool as well as a clinical method to ensure a sufficient dose has been deposited to cause adequate cell damage during the treatment. PPTT induced cell death can take place via apoptosis or necrosis depending on the laser dosage, exposure time and locations of nanoparticles inside the cell [40]. One of the first stages of damage is the loss of mitochondrial membrane integrity, and thereby, a loss of mitochondrial function [39]. Measurement of this functional status is possible as many of the important molecules in the respiratory chain are strong optical chromophores. However, tissue autofluorescence is relatively weak especially when a small-power light source is used to excite autofluorescence in a large tissue region.

We propose to address this problem in PPTT by exploiting the dual peaks of gold nanorods (GNRs) for conducting plasmonic photothermal treatment and enhancing weak cellular autofluorescence simultaneously, in which the later peak intensities indicate the progress of cell death during PPTT. While the peak of GNR in NIR can be used for treatment in PPTT as usual, the other peak in the visible region can be utilized for enhancing autofluorescence from NADH and FAD to facilitate the monitoring of treatment outcome. We demonstrate the use of PEGylated [41] GNRs

for photothermal therapy and track the cellular death by continuously measuring enhanced autofluorescence due to the encapsulation of the GNRs within live renal cell carcinoma cells [42].

2. Material and Methods

2.1 Preparation of gold nanorods and the cell line

Bare GNRs with an aspect ratio of 3.8 (10 *nm* in diameter and 38 *nm* in length) which had two plasmonic peaks at 765 *nm* and 520 *nm* , were purchased from Strem chemicals Inc. (Massachusetts, United States). The GNRs were delivered in water suspension with a concentration of about 6.68×10^{11} nanoparticles per *ml*. To make the nanorods biocompatible, the GNRs were PEGylated with mPEG (Sigma-Aldrich, Missouri, United States). The 1-μM mPEG solution was mixed with GNR suspension with a ratio of 1:4 and the mixture was incubated by constantly rotating using a tube rotator (Cole-Parmer, Illinois, United States) for 6, 12 and 24 hours in four different batches. Varying the time of incubation results in a range of thicknesses of PEG layer around the GNR. The PEGylated GNRs were separated from water by centrifuging, which were then washed with phosphate buffer solution (PBS). Finally, the PEGylated GNRs were re-suspended in PBS, which was later used for incubation with cells.

Human renal cell carcinoma cells (Caki-2 cell line) were purchased from American Type Culture Collection (Virginia, United States). Caki-2 cells were cultured in Iscove's Modified Dulbecco's Medium (IMDM) supplemented with 10% fetal bovine serum (FBS), and were incubated in the incubator at 37°*C* and with 5% CO_2. Cultures were maintained by the addition of or replacement by fresh medium every 3-4 days to maintain a cell density of 10^5-10^6 cells per *ml*. Since Caki-2 cell lines adhered to the surface of the culture flask during each passaging, the cells were gently scrapped from the surface and mixed well to separate the cells from each other before adding or replacing culture medium. A total of 1-*ml* cell suspension (around 10^6 cells) were then transferred to a 60 *mm* petridish, where they were mixed with PEGylated GNRs and incubated for another 24 hours in the

incubator. The PEGylated GNRs were washed once with culture medium prior to mixing with the caki-2 cell medium. After 24 hours, before scrapping the cells, the culture medium was removed and the petridish was replaced with PBS by washing the cells gently twice in PBS to get rid of GNRs in the extracellular matrix. The cells were then scrapped and used for further experiments. To evaluate cell death due to necrosis, 10 μl of 0.4% (*w/v*) trypan blue solution (Sigma-Aldrich, Missouri, United States) was added to 10 μl of the cell sample and mixed well. The mixture was left for 10-15 minutes in room temperature before the observation under optical microscope. Dead cells were stained blue while live cells remained unstained as their cytoplasm remained intact.

2.2 Experimental setup for plasmonic photothermal therapy and autofluorescence measurements

The schematic of the experimental setup showing the arrangement of the laser and thermocouple probe is shown in Fig. 1. A table top 500 *mW*, 785 *nm* laser (CNI laser, Changchun, China) was used for photothermal therapy. The FC fiber coupled laser was collimated using a fiber collimator (F240, Thorlabs, New Jersey, United States) with an NA of 0.5 and a focal length of 8 *mm*. The collimated beam diameter was about 6 *mm* that yielded a optical power density of about 5.14 W/cm^2. To measure temperature during photothermal therapy, a hypodermic T-type thermocouple with a diameter of 200 μm purchased from omega (HYPO, Connecticut, United States) was connected to a controller (NI 9211, National Instruments, Texas, United States), which was programmed using LabVIEW (National Instruments, Texas, United States) to record the temperature at desired time points. During experiments the thermocouple was placed in such a way that there was no direct illumination on the thermocouple by the 785 *nm* laser beam to ensure that the recorded temperature variation was solely due to the photothermal effect of laser illumination on cells.

Cells incubated with GNRs were prepared as described earlier before the start of the photothermal experiment. A cell sample of 0.5 *ml* was placed in a cuvette and exposed to the laser beam from the top as shown in Fig. 1. To prevent the cells from settling down during the experiment, which may result in non-uniform illumination of cells, the mixture was gently stirred using a

magnetic stirrer throughout the experiment. At every scheduled time point, an amount of 10-*µl* cell sample was taken out of the cuvette to be tested for viability. In each cell viability test, the 10-*µl* cell sample was mixed with 10 *µl* of 0.4% (*w/v*) trypan blue solution. The mixture was left for 10-15 minutes at room temperature before the observation under optical microscope. Dead cells were stained blue while live cells remained unstained as their cytoplasm remained intact. Meanwhile, another 120-*µl* cell sample was taken out and added to a 120-*µl* cuvette which was placed inside a commercial fluorescence spectrometer (LS-55, Perkin Elmer, Massachusetts, United States) to obtain autofluorescence spectrum. The autofluorescence emission spectrum between 450 *nm* and 600 *nm* that covered the emission peaks of NADH and FAD was recorded when the sample was illuminated with 405 *nm* excitation light. Prior to measuring the fluorescence, the dark spectrum was captured and the spectral values were subtracted from the actual experimental measurement at each wavelength.

2.3 Experimental design

The experiment was categorized into four groups in which the sample of cells incubated with GNRs was abbreviated as cells+GNRs for convenience. Out of the four groups, one was the experimental group consisting of cells+GNRs which was exposed to laser illumination (group 4) and the other three were control groups which were classified as cells+GNRs with no laser illumination (group 3), cells only exposed to laser (group 2) and cells only with no laser illumination as group 1. Experiments in each of these groups were carried out for 0, 2, 4, 6, 8 and 10 minutes with the continuous monitoring of temperature. For every time point, a new batch of fresh cells were used in the experiment. At the end of every experiment, autofluorescence was measured from all the four groups immediately and also cell viability test was carried out to determine the percentage of live cells. The entire set of experiments was repeated three times for every group.

The thermal damage due to varying laser exposure time was determined by measuring the autofluorescence and cell viability test at different stages of heating and was compared to the other

groups which involved less or no heating. Cell counting was done once for every one of three repititions for each cell sample in the study and was averaged whereas the autofluorescence intensity was averaged between ±10 *nm* from the peak emission wavelength of FAD (520 *nm*) and plotted against time for all the groups.

2.4 The Cell Damage Model

Cell damage due to thermal effect can be modeled as a first-order irreversible rate process equation [32, 43]

$$V \overset{k_c}{\rightarrow} D \tag{1}$$

where V represents the viable cells, D represents the injured or damaged cells, k_c is the cell damage rate. The cell viability after subjecting to temperature histories can be calculated using the below equation

$$C_v = \exp\left(-\int_0^{\tau} k_c \, dt\right) \tag{2}$$

where C_v is the cell viability after subjecting to a temperature $T(t)$, τ represents the treatment time (s), To calculate the damage rate the well known Arrhenius model [32] is considered which is as follows

$$k_c = A \times \tau \times exp\left(-\frac{E_a}{RT}\right) \tag{3}$$

where A is the frequency factor (s^{-1}), E_a is the activation energy ($J\ mol^{-1}$), and R is the universal gas constant (8.314 $J\ mol^{-1}\ K^{-1}$). The kinetic parameters for E_a and A for floating renal cell carcinoma were chosen as 287.49×10^3 $Jmol^{-1}$ and 4.362 s^{-1}, respectively [43]. The temperature values recorded at specific times during the therapy are used to calculate the thermal damage according to Eq. (2) and (3).

3. Results

Caki-2 cell lines and PEGylated GNRs were incubated for a maximum of 24 hours. After washing the incubated cells with GNRs with PBS to ensure the removal of extracellular GNRs, we could see a visible difference in the color of cells due to the presence of GNRs in the intracelluar matrix which entered the cells through endoscyotosis. The temperature change as a function of time for the experimental and control groups is as shown in Fig. 2(a). The control groups (1 and 3) were not exposed to the laser hence did not show any considerable changes in temperature. However, there was a slight increase in temperature in control group 2 that may be due to the heating of the medium by the 785 nm laser but this change in temperature was only about 2-3^{o}C after it was exposed for 10 minutes. The experimental group (group 4) showed a dramatic increase in the first 2 minutes and then a gradual increase in temperature with the time of laser illumination. At about 4 minutes of continuous exposure to the laser, the temperature began to reach the hyperthermic region and continued to do so until the end of the experiment.

At each scheduled time point, a small amount of cell samples taken out of cell suspension in all groups was mixed with trypan blue dye and a hematocytometer was used to determine the cell viability. The cell counting was done three times for one repetition on the same sample and was averaged. From Fig. 2(b), it is clear that only group 4 underwent cell death as compared to the control groups. In group 4, it can be observed that the cell death due to hyperthermia started to occur at 3-4 minutes. As the exposure time was increased further, the cell viability decreased faster until 8 minutes, at which the drop in the cell viability slowed down. The cell viability fell to nearly below 10% after an exposure to the laser light for 10 minutes.

Fig. 3(a) shows the calculated cell viability based on the recorded temperature at different points along with the experimental cell viability and autofluorescence data for Group 4. All the values in each curve have been divided by the maximum value in the same curve to achieve unity at time zero in order to facilitate comparison in the trend across curves. The data for other groups are

not shown because the calculated cell viability shows no change in the cell viability and remained 100%. At 6 minutes the calculated cell viability is around 57% as compared to 43% experimentally. After 10 minutes, the temperature eventually reaches $47.5^{o}C$, and the calculated cell viability drops to less than 17% as compared to less than 10% in the experimental study. This difference could be due to the proteolytic enzymes which is released by the cell when damaged which in turn damages the surrounding cells which is unaccounted for in the Arrhenius cell damage model. In contrast, the agreement between the experimental cell viability and measured autofluorescence is much better when the heating time is shorter than 4 minute. To further quantify the correlation between the experimental cell viability and the measured autofluorescence, the correlation graph between the two corresponding curves in Fig. 3(a) is shown in Fig. 3(b). The high correlation coefficient, 0.99, indicates the strong positive correlation between the quantities, which suggests the possibility of monitoring cell viability continuously by measuring autofluorescence.

The autofluorescence spectra from all the groups were measured immediately after the start of experiments until the end of the experiment. The last set of spectra measured 10 minutes after the start of the experiments as shown in Fig. 4(a). It can be observed that there was a two fold increase in the autofluorescence from cells+GNRs (No Laser) group as compared to only cells (No Laser group), which should be due to fluorescence enhancement caused by GNR. In addition to the field enhancement by the GNRs, the radiative decay rate of the autofluorescing molecule increases when molecules are placed a few nanometers away from GNRs resulting in additional fluorescence enhancement [44].

The autofluorescence spectra measured at all time points were then processed to determine the progress of cell death at different stages of heating in the experimental group compared to the other groups which involved less or no heating. The fluorescence intensity was averaged around the peak emission wavelength of FAD (520 *nm*) for a bandwidth of 20 *nm* and plotted against time for all the groups as shown in Fig. 4(b). In the experimental group, it can be observed that the intensity

decreased as the therapy progressed and it followed a similar trend as that of cell viability in Fig. 2(b). Group 3 (Cells+GNRs, No Laser) showed an increase of two folds relative to Group 1 (Cells only, No Laser) in the initial autofluorescence emission intensity due to the presence of GNRs inside the cells resulting in fluorescence enhancement, which was also observed in Fig. 4(a).

PEGylation has become a standard procedure and a commonly used procedure to make the nanoparticles biocompatible. A few of the US FDA approved PEGylated nanoparticles are already used in preclinical applications. PEGylation not only makes the NP biocompatible but also can be tailored for target specific binding when used for *in vivo* studies thus reducing the accumulation of NP in the liver and spleen [41]. GNR-PEG shows high stability in biological media and low cytotoxicity in non-cancer cells [45]. Therefore it is expected that the PEG-GNR used in this study would demonstrate similar effects to non-cancer cells as to cancer cells shown in Fig. 7 in the cases of with and without laser illumination. The PEGylation also acts as a spacer layer facilitating fluorescence enhancement [46]. The optimal distance between the fluorophore and the plasmonic nanoparticle for fluorescence enhancement was shown in a range of 5-10 *nm* [47] in synthetic samples. To find the optimal parameter of the PEGylation layer in cells in this study, we have varied the thickness of the PEGylation layer by incubating the mPEG (50 μM) and GNR solution (6.68×10^{11} nanoparticles/ *ml*) mixture (1:4 ratio) for 6, 12 and 24 hours. The PEG layer thickness was later measured using Transmission Electronic Microscope (TEM). Fig. 5 shows the TEM images of the GNRs without and with the PEGylation layer as the PEGylation duration was increased from 6 to 12 and then to 24 hours. As the duration of incubation increased the PEG layer thickness also increased as seen in Fig. 5. For longer duration (24 hours), it can be noticed that there was GNR aggregation. Approximately, a PEG layer with a thickness of 2, 5 and 10 *nm* was formed when the mixture was rotated for 6, 12 and 24 hours, respectively.

To observe the effect of the spacer layer thickness on the autofluorescence emission from cells, GNRs with PEG layers of varying thicknesses were incubated with cells for 24 hours under ideal

conditions. The autofluorescence images of cells, in which the excitation wavelength was 405 *nm* and the emission filter covered a pass band of 450 *nm* to 600 *nm*, at 40× magnification were captured as shown in Fig. 6. The cells with no GNRs was hardly visible as compared to cells with PEGylated GNRs. Cells that were incubated with the GNRs coated by a 5-*nm* or 10-*nm* PEGylation layer showed higher autofluorescence intensity as compared to those with the GNRs coated by a 2-*nm* PEG layer.

4. Discussion

When the GNRs are incubated with cells, they are endocytosed by cells through a process called receptor-mediated endocytosis (RME) which occurs via interactions between proteins on the surface of nanoparticles and cell membrane receptors. However, for bare nanoparticles, the proteins in the culture medium get attached to the nanoparticle surface during incubation resulting in RME [48-50]. Nanoparticles less than 50 *nm* exhibit higher uptake as compared to larger nanoparticles [51]. The GNRs used in this study had an aspect ratio of 3.8 that was relatively small and the total size of the GNR was small too with a longitudinal size of 38 *nm* (±10%). Chithrani *et al* [52] have showed that the smaller the aspect ratio and size are, the higher the uptake will be. Under laser illumination these GNRs convert light to heat and cause localized hyperthermia. The measured temperature in the treatment group reached a maximum of about $47.5^{o}C$ after laser exposure for 10 minutes. In the present study, the cell death can be primarily attributed to necrosis due to the sudden increase in temperature in the first 4 minutes which reaches the hyperthermic region which in turn results in cell membrane disruption [53, 54] allowing the trypan blue to enter the necrotic cell. At longer durations of laser exposure when temperature steadily increases, the cell viability decreases to as much as 40 % at 6 mins as observed in fig. 2(b) as a result of necrosis. However, cell death due to apoptosis may be negligible since cell apoptosis becomes significant only when the cells are exposed for at least 30 mins at enhanced temperature between $42^{o}C$ and $44^{o}C$ [53]. Hence the change in autofluorescence was primarily a result of necrosis. This phenomenon was confirmed by cell imaging

results in Fig. 7(a) and 7(b). It can be observed that the laser exposed section, i.e. the top portion of the figure, of gold nanorods internalized cells showed nearly no autofluorescence in Fig. 7(a) and the cells appear blue when stained with trypan blue in Fig. 7(b). The latter observation suggests that cells exposed to the laser underwent necrosis. In contrast, the cells that were not treated by laser illumination, i.e. the bottom portion of the figure, showed strong autofluorescence in Fig. 7(a) and no blue color in Fig. 7(b).

According to Fig. 3(a), the autofluorescence closely follows the cell viability curve as compared to the calculated value, this deviation of the calculated viability curve from the experimental curve may be due to the release of proteolytic enzymes which damage surrounding cells when necrosis occur which is unaccounted for in the Arrhenius cell damage model. In the temperature range of 41-47 ^{o}C the cell undergoes several macromolecular changes and affects the functions in almost all the cellular compartments. In particular, hyperthermia causes the denaturation of proteins in microsomal membranes, mitochondria, cytosol, nuclei and nuclear matrices also disrupts the biomolecular assemblies in the nucleus and cell membrane [25, 55, 56] which eventually leads to cell death. The decrease in the measured autofluorescence intensity of the treated cells as shown in Fig. 4(a) and (b) was due to the mitochondrial damage resulting in the alteration in the redox status of cells [57]. The autofluorescence intensity of the therapy group in Fig. 4(a) signifies that the cells have been damaged followed by the reduction in the autofluorescence intensity. This is the mechanism behind the use of cellular autofluorescence for the monitoring of cell viability variation in photothermal therapy. One additional advantage of using autofluorescence to monitor the treatment outcome in plasmonic photothermal therapy involving GNRs is that the relatively weak cell autofluorescence can be enhanced by GNRs, which could increase the sensitivity of this technique to the variation in cell viability.

In Fig. 4(a) and (b), it is noticed that there is a nearly twice increase in the autofluorescence intensity from cells with GNRs as compared to cells without GNRs. The PEGylation layer on the

nanorods was about 5 *nm*. The enhanced absorption and scattering properties of the GNRs results in strong amplified local electromagnetic field which in turn influences the nearby autofluorescence molecule resulting in fluorescence enhancement. Plasmonic enhancement of fluorescence requires the fluorophore molecules in the close proximity to the metal nanoparticle. However, fluorophores located extremely close to or in direct contact with the nanoparticle surface quenches the fluorescence emission due to a nonradiative energy transfer between the excited state of the fluorescing molecules and the metal nanoparticle [58]. El-Sayed *et al* [59] showed the autofluorescence from NADH suspension was quenched in the presence of bare gold nanospheres (GNSs) and GNRs (no surface modification) which was attributed to the re-absorption of the emitted field. The presence of GNRs in the extracellular matrix of live cells also resulted in quenching effect due to the distance between the cellular enzymes and proteins. Therefore an optimal distance from the metal nanoparticle is necessary at which the fluorescence emission intensity can be maximally enhanced [58]. Fig. 6 shows that as the PEGylation layer is increased from 2 *nm* (PEG: 6 hours) to 5 *nm* (PEG: 12 hours) there is a significant increase in the peak fluorescence intensity. However, there is no significant change in the peak fluorescence intensity when the PEGylation layer is increased from 5 *nm* (PEG: 12 hours) to 8-10 *nm* (PEG: 24 hours). This agrees with the findings in another study using synthetic samples in the literature [47]. This could be attributed to the observation in Fig. 6 that the GNRs tend to aggregate after PEGylation for 24 hours. The aggregation may cause difficulty for GNRs to get into cells and approach endogenous fluorophore molecules in mitochondria.

To our knowledge, the enhancement of cellular autofluorescence has not been reported but the effect of metal island films on the autofluorescence enhancement from the suspensions of NADH (10 times) and FAD (5 times) have been reported [59, 60] with a 5-*nm* spacer layer. As compared to these reports the two time enhancement is considered small. The potential reasons for the small enhancement factor of 2 may be due to: (i) the weaker plasmonic peak of the GNR in the visible region; (ii) the strong plasmon field around the GNR may not be sufficiently close to the endogenous fluorophore and (iii) the nanorods may tend to aggregate inside the cell resulting in the

red shift of its plasmonic peaks [61]. The enhancement factor can be improved by using nanoparticles with strong plasmonic peak in the visible region and exploiting the targeted binding of GNRs to the mitochondria so as to make the endogenous fluorophore close to the strong plasmonic field generated by the nanoparticle.

The effect of exposure time on the temperature rise and cell death can be observed in Fig. 2(a) and (b). It is interesting to note that only when the temperature reaches the hyperthermic region (>43^{o}C) at 4 minutes and beyond, one starts to see significant drop in cell viability. More than 50% cells are dead at 6 minutes which steadily increases as the exposure time is increased in Group 4 in Fig. 2(b). It is important to observe that the measurement of autofluorescence intensity as shown in Fig. 4(b) follows the same trend as that of cell viability in Fig. 2(b). In the first 2 minutes when the temperature reaches 3^{o}C above the normal temperature, the autofluorescence intensity drops by less than 5% compared to that in control group 3, which clearly indicates that there is no major cell death. However, as the temperature steadily rises to 6^{o}C above normal, the autofluorescence intensity decreases to about 54.5% at 6 minutes as compared to control group 3. To further quantify the correlation between the thermal damage profile and the autofluorescence profile, the correlation coefficient between the curve shown in Fig. 2(b) and that shown in Fig. 4(b) both for Group 4 was calculated and found that the value was 0.99. The high correlation coefficient, close to 1, indicates that the validity of using autofluorescence to replace the thermal damage value for the monitoring of cell viability.

The findings in the current *in vitro* study could be extended to the *in vivo* study. Because of the leaky vasculature in a solid tumor, PEGylated nanorods are retained and distributed in a volume of the tumor due to the enhanced permeability and retention (EPR) effect when these nanorods are injected intravenously or intraperitoneally. The same volume will be illuminated by a therapy laser or monitoring laser in photothermal therapy. The cell suspension used in this study mimics such a tissue volume. The difference between the cell suspension and an actual solid

tumor is cell density. The trends in tissue viability and fluorescence intensity observed in this study will be directly applicable to the superficial tissue region in a solid tumor since there is little light attenuation. In a deep tissue region of the solid tumor, light absorption and scattering will be much stronger due to a much greater cell density. Therefore the attenuation of treatment radiation or fluorescence will be dramatically larger. However, the enhancement of fluorescence due to PEG-GNR relative to the fluorescence without it should remain unchanged since light attenuation is identical in two cases and only the excited fluorescence is enhanced. The similar reasoning is applicable to the effect of therapeutic light propagation. The results in this study show that apart from enhancing light absorption to facilitate plasmonic photothermal therapy, GNRs can also be used for enhancing the relatively weak cell autofluorescence that can serve as a direct indicator of cell viability. If cell autofluorescence is measured quickly during therapy, one can determine the progress of the treatment online by just monitoring the autofluorescence intensity and thus eliminating the need of performing the time consuming and tedious cell viability test to determine the cell treatment outcome. The continuous monitoring of autofluorescence can help optimize the treatment outcome in real time by providing instant feedback for the fine adjustment of laser dosage using those methods reported previously [33, 34] after adoption for fast computation.

Conclusion

Plasmonic photothermal therapy on gold nanorods internalised Caki-2 cell lines was performed. The results show the steady rise in temperature due to light to heat conversion effect of nanorods when continuously illuminated with near infrared laser. The autofluorescence measurement and cell viability test reveals the progress of cell death when the temperature reached the hyperthermic region. The autofluorescence measurement and cell viability test show a similar trend over the duration of laser exposure. Apart from nanorods assisting the laser therapy of cancer cells it also enhanced the weak autofluorescence by 2 times. The PEGylation layer also plays a significant role in

the enhancement factor as the thickness reduces the enhancement reduces. By specific binding of nanorods to the mitochondria within the cell may results in higher enhancement. Continuous monitoring of the autofluorescence can predict the progress of cell death during plasmonic photothermal therapy thus eliminating the need for alternative time consuming and off-line cell staining techniques to determine cell death.

Acknowledgements

The authors would like to acknowledge financial support from ASTAR-ANR joint grant (Grant no. 102 167 0115) and ASTAR-PSF grant (Grant no. 122-PSF-0012) funded by ASTAR-SERC in Singapore.

References

1. Huang, X., et al., *Plasmonic photothermal therapy (PPTT) using gold nanoparticles.* Lasers in medical science, 2008. **23**(3): p. 217-28.
2. Huang, X.H., et al., *Cancer cell imaging and photothermal therapy in the near-infrared region by using gold nanorods.* Journal of the American Chemical Society, 2006. **128**(6): p. 2115-2120.
3. Dickerson, E.B., et al., *Gold nanorod assisted near-infrared plasmonic photothermal therapy (PPTT) of squamous cell carcinoma in mice.* Cancer Lett, 2008. **269**(1): p. 57-66.
4. Choi, W.I., et al., *Photothermal Cancer Therapy and Imaging Based on Gold Nanorods.* Annals of Biomedical Engineering, 2012. **40**(2): p. 534-546.
5. Nima, Z.A., et al., *Circulating tumor cell identification by functionalized silver-gold nanorods with multicolor, super-enhanced SERS and photothermal resonances.* Scientific Reports, 2014. **4**.
6. Mackey, M.A., et al., *The Most Effective Gold Nanorod Size for Plasmonic Photothermal Therapy: Theory and In Vitro Experiments.* Journal of Physical Chemistry B, 2014. **118**(5): p. 1319-1326.
7. Loo, C., et al., *Nanoshell-enabled photonics-based imaging and therapy of cancer.* Technol Cancer Res Treat, 2004. **3**(1): p. 33-40.
8. Hirsch, L.R., et al., *Nanoshell-mediated near-infrared thermal therapy of tumors under magnetic resonance guidance.* Proc Natl Acad Sci U S A, 2003. **100**(23): p. 13549-54.
9. Lin, A.W.H., et al., *Nanoshells for integrated diagnosis and therapy of cancer.* Nanosensing: Materials and Devices, 2004. **5593**: p. 308-316.
10. Bardhan, R., et al., *Nanoshells with Targeted Simultaneous Enhancement of Magnetic and Optical Imaging and Photothermal Therapeutic Response.* Advanced Functional Materials, 2009. **19**(24): p. 3901-3909.
11. Gobin, A.M., et al., *Near-infrared resonant nanoshells for combined optical imaging and photothermal cancer therapy.* Nano Letters, 2007. **7**(7): p. 1929-1934.
12. Vo-Dinh, T., et al., *Plasmonic nanoprobes: from chemical sensing to medical diagnostics and therapy.* Nanoscale, 2013. **5**(21): p. 10127-10140.
13. Mayoral, A., et al., *Polyhedral shaped gold nanoparticles with outstanding near-infrared light absorption.* Applied Physics a-Materials Science & Processing, 2009. **97**(1): p. 11-18.
14. Wang, S., et al., *Single continuous wave laser induced photodynamic/plasmonic photothermal therapy using photosensitizer-functionalized gold nanostars.* Adv Mater, 2013. **25**(22): p. 3055-61.
15. Chen, J.Y., et al., *Gold Nanocages as Photothermal Transducers for Cancer Treatment.* Small, 2010. **6**(7): p. 811-817.
16. Skrabalak, S.E., et al., *Gold nanocages for cancer detection and treatment.* Nanomedicine, 2007. **2**(5): p. 657-668.
17. Chen, J.Y., et al., *Immuno gold nanocages with tailored optical properties for targeted photothermal destruction of cancer cells.* Nano Letters, 2007. **7**(5): p. 1318-1322.
18. Au, L., et al., *A quantitative study on the photothermal effect of immuno gold nanocages targeted to breast cancer cells.* Acs Nano, 2008. **2**(8): p. 1645-1652.
19. Krishnan, S., P. Diagaradjane, and S.H. Cho, *Nanoparticle-mediated thermal therapy: Evolving strategies for prostate cancer therapy.* International Journal of Hyperthermia, 2010. **26**(8): p. 775-789.
20. Goodrich, G.P., et al., *Photothermal therapy in a murine colon cancer model using near-infrared absorbing gold nanorods.* Journal of Biomedical Optics, 2010. **15**(1).
21. Rayavarapu, R.G., et al., *Synthesis, functionalization and characterization of rod-shaped gold nanoparticles as potential optical contrast agents*, in *Molecular Imaging*, K. Licha and V. Ntziachristos, Editors. 2007. p. U42-U51.

22. Wang, J., et al., *Selective photothermal therapy for breast cancer with targeting peptide modified gold nanorods.* Dalton Transactions, 2012. **41**(36): p. 11134-11144.
23. Gormley, A.J., et al., *Plasmonic photothermal therapy increases the tumor mass penetration of HPMA copolymers.* J Control Release, 2013. **166**(2): p. 130-8.
24. Ungureanu, C., et al., *Light Interactions with Gold Nanorods and Cells: Implications for Photothermal Nanotherapeutics.* Nano Letters, 2011. **11**(5): p. 1887-1894.
25. Roti, J.L.R., *Cellular responses to hyperthermia (40-46 degrees C): Cell killing and molecular events.* International Journal of Hyperthermia, 2008. **24**(1): p. 3-15.
26. Maksimova, I.L., et al., *Near-infrared laser photothermal therapy of cancer by using gold nanoparticles: Computer simulations and experiment.* Medical Laser Application, 2007. **22**(3): p. 199-206.
27. Chen, Y., et al., *Magnetic resonance imaging guidance for laser photothermal therapy.* J Biomed Opt, 2008. **13**(4): p. 044033.
28. Lal, S., S.E. Clare, and N.J. Halas, *Nanoshell-enabled photothermal cancer therapy: impending clinical impact.* Acc Chem Res, 2008. **41**(12): p. 1842-51.
29. O'Neal, D.P., et al., *Photo-thermal tumor ablation in mice using near infrared-absorbing nanoparticles.* Cancer Lett, 2004. **209**(2): p. 171-6.
30. Lal, S., S.E. Clare, and N.J. Halas, *Nanoshell-Enabled Photothermal Cancer Therapy: Impending Clinical Impact.* Accounts of Chemical Research, 2008. **41**(12): p. 1842-1851.
31. Day, E.S., et al., *Nanoshell-mediated photothermal therapy improves survival in a murine glioma model.* Journal of Neuro-Oncology, 2011. **104**(1): p. 55-63.
32. Henriques, F.C., *Studies of Thermal Injury .5. The Predictability and the Significance of Thermally Induced Rate Processes Leading to Irreversible Epidermal Injury.* Archives of Pathology, 1947. **43**(5): p. 489-502.
33. Kannadorai, R.K. and Q. Liu, *Optimization in interstitial plasmonic photothermal therapy for treatment planning.* Med Phys, 2013. **40**(10): p. 103301.
34. Xu, X.A., A. Meade, and Y. Bayazitoglu, *Numerical investigation of nanoparticle-assisted laser-induced interstitial thermotherapy toward tumor and cancer treatments.* Lasers in Medical Science, 2011. **26**(2): p. 213-222.
35. Li, L.Z., et al., *Mitochondrial Redox Imaging for Cancer Diagnostic and Therapeutic Studies.* Journal of Innovative Optical Health Sciences, 2009. **2**(4): p. 325-341.
36. Zhang, Z.H., et al., *Redox ratio of mitochondria as an indicator for the response of photodynamic therapy.* Journal of Biomedical Optics, 2004. **9**(4): p. 772-778.
37. Liu, Q., et al., *Compact point-detection fluorescence spectroscopy system for quantifying intrinsic fluorescence redox ratio in brain cancer diagnostics.* Journal of Biomedical Optics, 2011. **16**(3): p. 037004.
38. Liu, Q. and T. Vo-Dinh, *Spectral filtering modulation method for estimation of hemoglobin concentration and oxygenation based on a single fluorescence emission spectrum in tissue phantoms.* Medical Physics, 2009. **36**(10): p. 4819-4829.
39. Wang, H.W., Y.H. Wei, and H.W. Guo, *Reduced Nicotinamide Adenine Dinucleotide (NADH) Fluorescence for the Detection of Cell Death.* Anti-Cancer Agents in Medicinal Chemistry, 2009. **9**(9): p. 1012-1017.
40. Xiaohua Huang, M.A.E.-S., *Plasmonic photo-thermal therapy (PPTT).* Alexandria Journal of Medicine, 2011(47): p. 1-9.
41. Jokerst, J.V., et al., *Nanoparticle PEGylation for imaging and therapy.* Nanomedicine, 2011. **6**(4): p. 715-728.
42. Acquavella, N. and T. Fojo, *Renal Cell Carcinoma: Trying but Failing to Improve the Only Curative Therapy.* Journal of Immunotherapy, 2013. **36**(9): p. 459-461.
43. He, X.M. and J.C. Bischof, *The kinetics of thermal injury in human renal carcinoma cells.* Annals of Biomedical Engineering, 2005. **33**(4): p. 502-510.

44. Lakowicz, J.R., *Radiative decay engineering: biophysical and biomedical applications.* Analytical Biochemistry, 2001. **298**(1): p. 1-24.
45. Grabinski, C., et al., *Effect of Gold Nanorod Surface Chemistry on Cellular Response.* Acs Nano, 2011. **5**(4): p. 2870-2879.
46. Guo, S.-H., et al., *Spacer Layer Effect in Fluorescence Enhancement from Silver Nanowires over a Silver Film; Switching of Optimum Polarization.* Nano Letters, 2009. **9**(7): p. 2666-2670.
47. Kulakovich, O., et al., *Enhanced luminescence of CdSe quantum dots on gold colloids.* Nano Letters, 2002. **2**(12): p. 1449-1452.
48. Mukherjee, S., R.N. Ghosh, and F.R. Maxfield, *Endocytosis.* Physiological Reviews, 1997. **77**(3): p. 759-803.
49. Kirchhausen, T., *Three ways to make a vesicle.* Nature Reviews Molecular Cell Biology, 2000. **1**(3): p. 187-198.
50. Jin, H., et al., *Size-Dependent Cellular Uptake and Expulsion of Single-Walled Carbon Nanotubes: Single Particle Tracking and a Generic Uptake Model for Nanoparticles.* Acs Nano, 2009. **3**(1): p. 149-158.
51. Chithrani, D.B., *Intracellular uptake, transport, and processing of gold nanostructures.* Molecular Membrane Biology, 2010. **27**(7): p. 299-311.
52. Chithrani, B.D., A.A. Ghazani, and W.C.W. Chan, *Determining the size and shape dependence of gold nanoparticle uptake into mammalian cells.* Nano Letters, 2006. **6**(4): p. 662-668.
53. Harmon, B.V., et al., *Cell-Death Induced in a Murine Mastocytoma by 42-47-Degrees-C Heating Invitro - Evidence That the Form of Death Changes from Apoptosis to Necrosis above a Critical Heat Load.* International Journal of Radiation Biology, 1990. **58**(5): p. 845-858.
54. Zhou, J.M., et al., *Effect of hyperthermia on the apoptosis and proliferation of CaSki cells.* Molecular Medicine Reports, 2011. **4**(1): p. 187-191.
55. Huff, T.B., et al., *Hyperthermic effects of gold nanorods on tumor cells.* Nanomedicine, 2007. **2**(1): p. 125-132.
56. Lepock, J.R., *Cellular effects of hyperthermia: relevance to the minimum dose for thermal damage.* International Journal of Hyperthermia, 2003. **19**(3): p. 252-266.
57. Dressler, C., et al., *Fluorescence imaging of heat-stress induced mitochondrial long-term depolarization in breast cancer cells.* Journal of Fluorescence, 2006. **16**(5): p. 689-695.
58. Anger, P., P. Bharadwaj, and L. Novotny, *Enhancement and Quenching of Single-Molecule Fluorescence.* Physical Review Letters, 2006. **96**(11).
59. El-Sayed, I., et al., *Effect of plasmonic gold nanoparticles on benign and malignant cellular autofluorescence: A novel probe for fluorescence based detection of cancer.* Technology in Cancer Research & Treatment, 2007. **6**(5): p. 403-412.
60. Chowdhury, M.H., J.R. Lakowicz, and K. Ray, *Ensemble and Single Molecule Studies on the Use of Metallic Nanostructures to Enhance the Intrinsic Emission of Enzyme Cofactors.* Journal of Physical Chemistry C, 2011. **115**(15): p. 7298-7308.
61. El-Sayed, I.H., X.H. Huang, and M.A. El-Sayed, *Surface plasmon resonance scattering and absorption of anti-EGFR antibody conjugated gold nanoparticles in cancer diagnostics: Applications in oral cancer.* Nano Letters, 2005. **5**(5): p. 829-834.

Figures

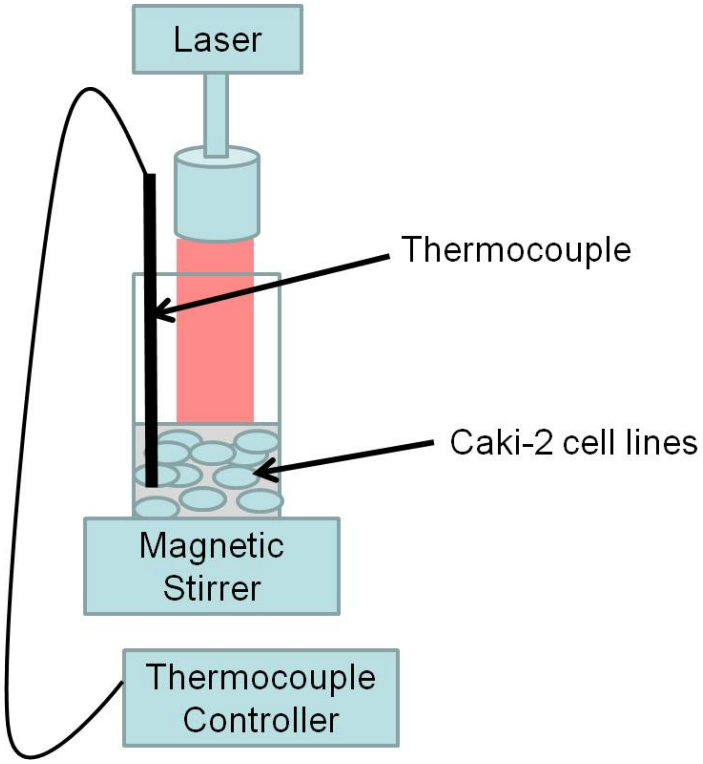

Figure 1: Schematic of the experimental setup showing the location of thermocouple and 785 *nm* therapy laser into the cell suspension which is gently stirred constantly preventing it from settling down.

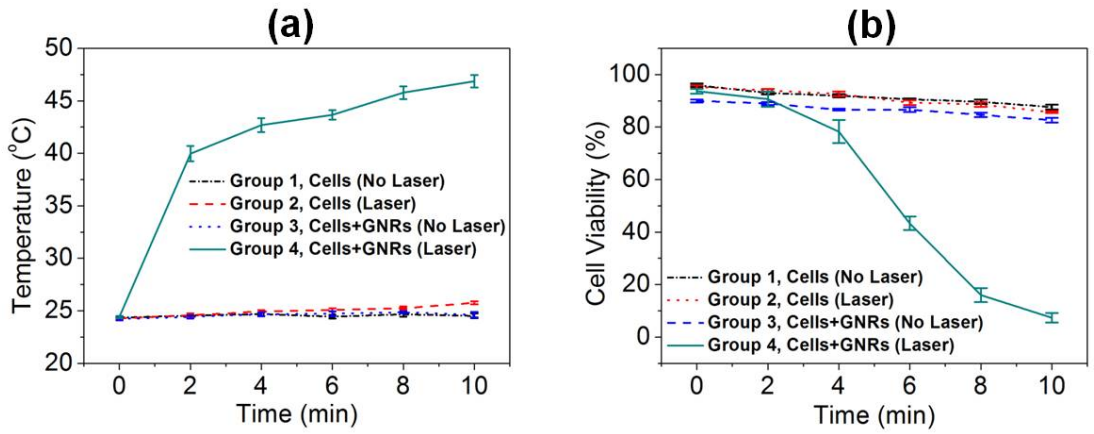

Figure 2: Temperature and cell viability measured in the treatment and control groups. (a) Temperature as a function of time. (b) Cell viability as a function of time.

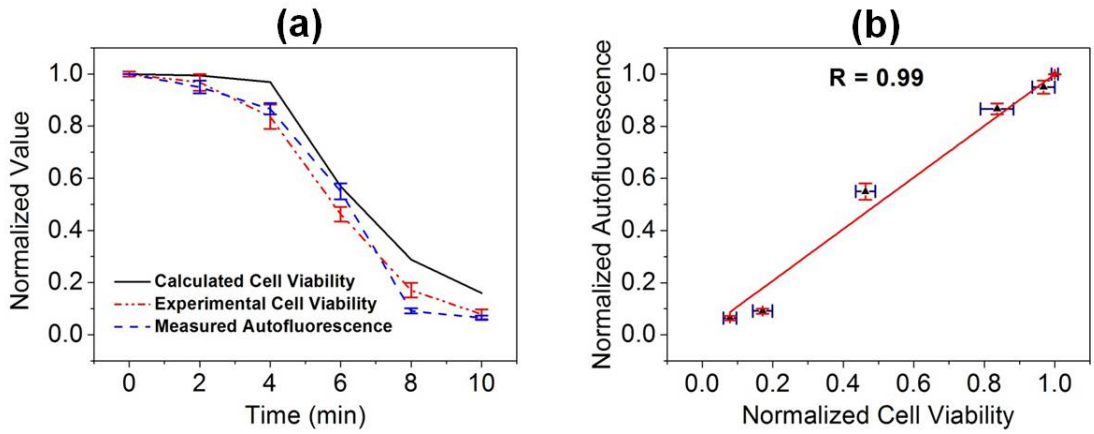

Figure 3. (a) Comparison of calculated cell viability based on Arrhenius model, the experimental cell viability and the measured autofluorescence as a function of time. (b) The correlation between cell viability and autofluorescence showing high correlation coefficient R between the two quantities. Note all data were obtained in Group 4.

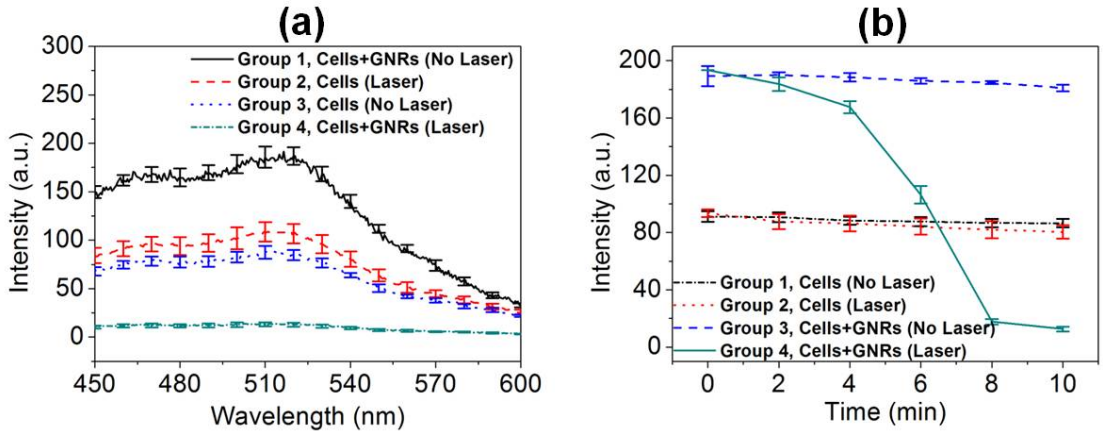

Figure 4: Autofluorescence measurements. (a) Autofluorescence emission spectra of the treatment and control groups measured 10 *min* after the start of the experiments. (b) Average cell autofluorescence intensity at the FAD peak (520 ±10 *nm*) as a function of time from the start of the experiments in the treatment and control groups .

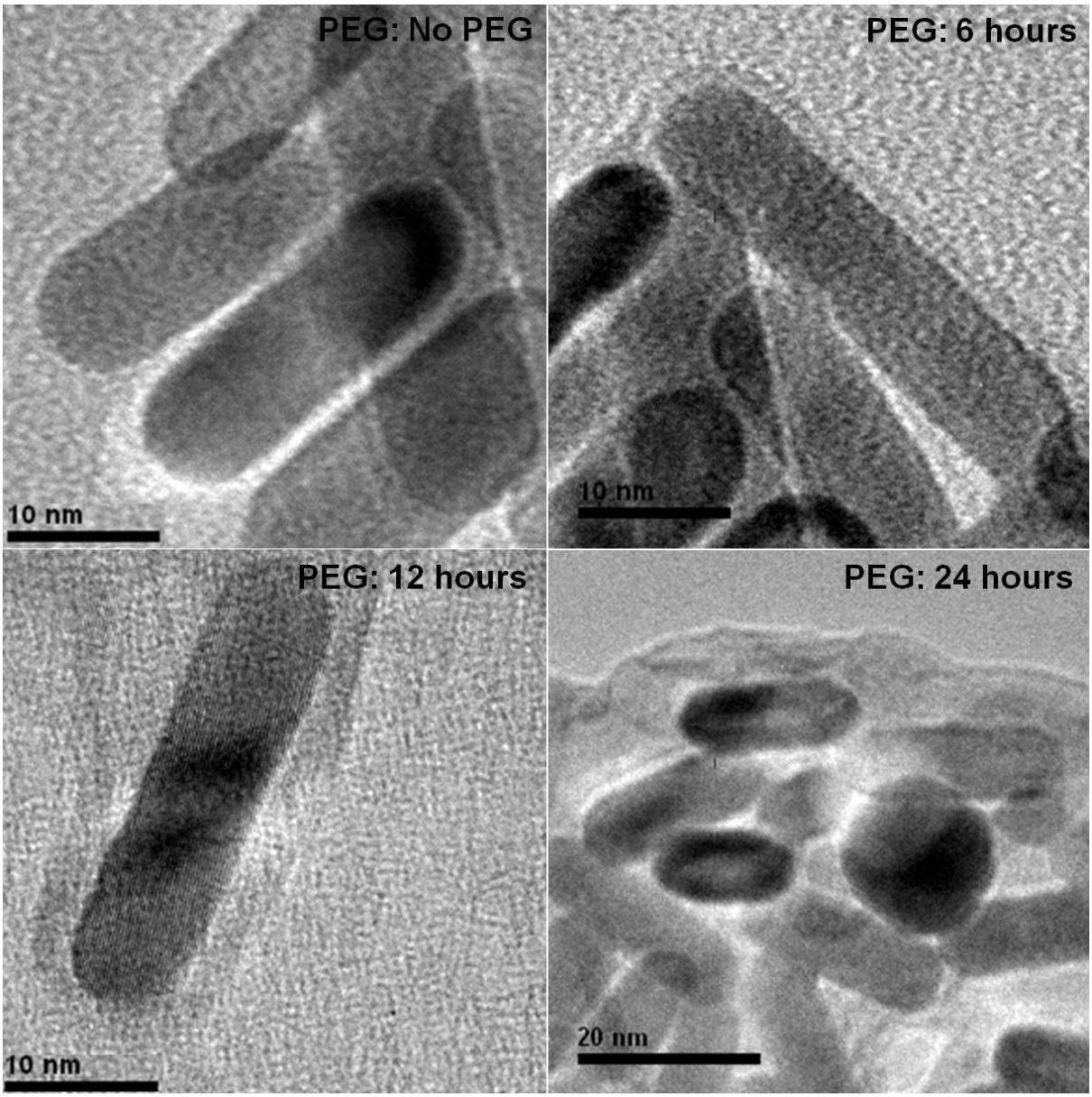

Figure 5: TEM images of the gold nanorods (GNR) without and with the PEGylation layer as the PEGylation duration was increased from, 6 to 12 and then to 24 hours. The PEG: 24 hours image is zoomed out (scale bar 20 *nm*) to show the aggregation of GNRs.

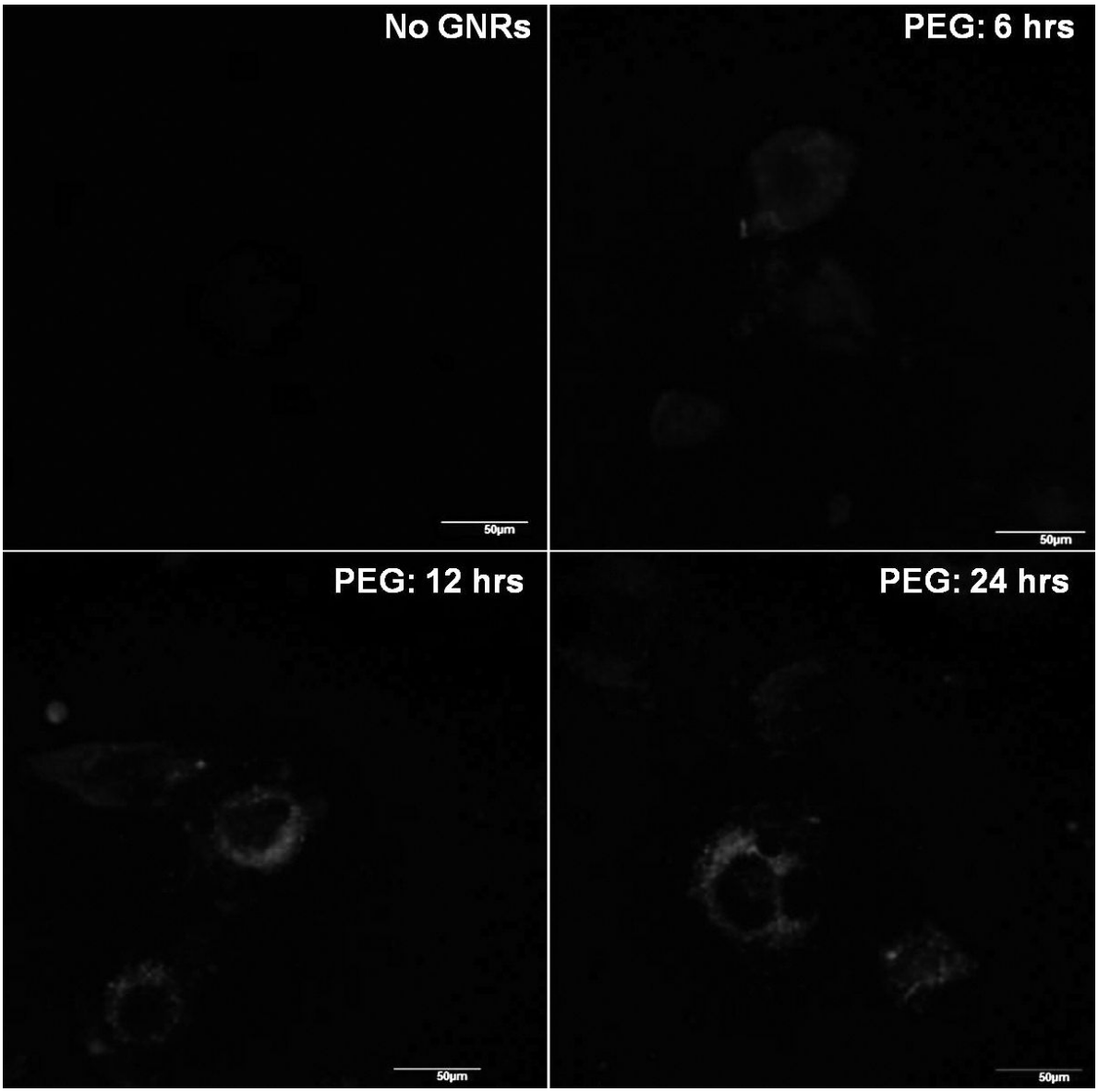

Figure 6: Confocal fluorescence images of cells captured at 40× magnification illuminated at 405 *nm* laser and the emission was collected from 450 to 600 *nm* wavelength range. The scale bar represents 50 μm.

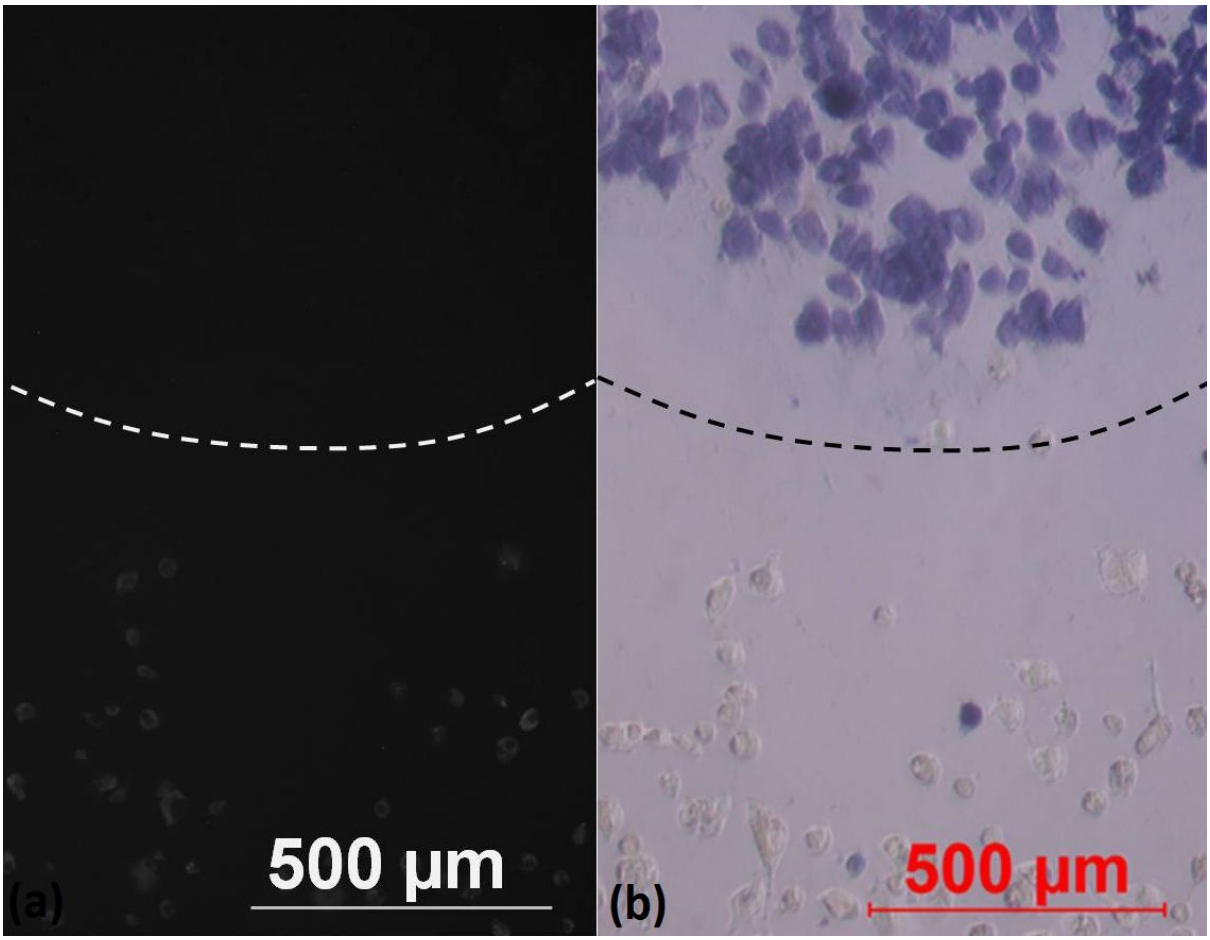

Figure 7: (a) Autofluorescence Image of unstained cells that internalised the GNR for 24 hours, in which cells on top of the dashed line were treated by 10-min constant laser illumination and those below the dashed line were not treated. (b) Brightfield image of the same cells stained by trypan blue to highlight necrotic cells. Autofluorescence image of cells were captured at 5× magnification, in which the excitation wavelength was from a white light source with a bandpass filter at 436±10 *nm* and the emission band was ranged from 535 ± 15 *nm*.